A Comprehensive Study of the Reaction $NH_2 + NO \rightarrow$ Products: Reaction Rate Coefficients, Product Branching Fractions, and *ab Initio* Calculations

M. Wolf,[†] D. L. Yang,[‡] and J. L. Durant*

Combustion Research Facility, Sandia National Laboratories, Livermore, California 94551

Received: April 16, 1997; In Final Form: June 10, 1997[⊗]

We have undertaken a comprehensive study of the reaction $NH_2(X^2B_1) + NO \rightarrow N_2 + H_2O$ (1a) and $NH_2(X^2B_1) + NO \rightarrow N_2H + OH \rightarrow N_2 + H + OH$ (1b). Experimental measurements of the reaction rate coefficient and product branching fraction are combined with accurate ab initio calculations to give a detailed picture of this important reaction. The rate constant of reaction 1 was investigated in the temperature range 203 K $\leq T \leq$ 813 K using the laser photolysis/CW laser-induced fluorescence technique for production and detection of NH_2. The rate coefficient was found to be pressure independent between 10 and 100 Torr and is well described by $k_1(T) = 1.65 \times 10^{-7} T^{-1.54} \exp(-93\ \mathrm{K}/T)$ cm^3/(molecule·s). The deuterium kinetic isotope effect for the reactions of NH_2 and ND_2 with NO was investigated at temperatures between 210 and 481 K. A small, temperature-independent isotope effect of $k_H/k_D = 1.05 \pm 0.03$ was found. Additional experimental work focused on measuring the product branching fraction for production of OH, Φ_{1b}, and its deuterium isotope effect at room temperature. Measurements were performed using the discharge-flow technique with mass spectrometric detection of products. OH from channel 1b was reacted with excess CO and measured as CO_2. The room temperature branching fraction was measured as $\Phi_{1b} = 9.0 \pm 2.5\%$ ($NH_2 + NO$; $T = 298$ K) and $\Phi_{1b} = 5.5 \pm 0.7\%$ ($ND_2 + NO$; $T = 298$ K). Theoretical calculations have characterized the stationary points on the potential energy surface connecting reactants with products using G2 and G2Q levels of theory. These calculations support the experimentally observed temperature dependences and kinetic isotope effects.

Introduction

In the thermal DeNOx process the reaction of NH_2 with NO is a primary destruction mechanism for nitric oxide. Knowledge of its rate and branching fraction into the possible product channels

$$NH_2(X^2B_1) + NO \rightarrow N_2 + H_2O \qquad (1a)$$

$$\rightarrow N_2H + OH \rightarrow N_2 + H + OH \qquad (1b)$$

is of central importance in the successful modelling of the thermal $DeNO_x$ process.[1] Channel 1a is chain terminating, and for the $DeNO_x$ process to be self-sustaining at least part of the reactive flux must go through channel 1b. The lifetime of N_2H formed in channel 1b has been a source of considerable controversy over the years, but it is now generally agreed that the lifetime of N_2H is short, in keeping with experimentally measured upper limits[2] and theoretically calculated lifetimes.[3−5]

In the atmosphere, NH_2 is generated from ammonia from either photolysis or reaction with OH radicals.[6] Although production of NH_2 from NH_3 is probably only a small loss channel,[7] the flux of NH_3 into the atmosphere is quite large,[8] and its reactions with atmospheric species need to be considered. Since NH_2 does not react with N_2 and reacts only very slowly with O_2,[9] reactions with trace species, such as NO, could be important, especially in polluted urban environments.

The reaction of NH_2 with NO is an association reaction with multiple product channels available to the initially formed adduct. The existence of energetically accessible product channels should result in little of the initially produced adduct being able to redissociate to reactants, and hence the reaction rate coefficients are expected to be pressure independent. The potential energy surface explored by this reaction is complicated by the presence of energetically accessible H-atom migrations and cis-trans isomerizations connecting multiple stable intermediates. Production of $N_2 + H_2O$ products requires breaking of all of the bonds present in the reactants and forming all of the bonds present in the products, highlighting the complexity of this elementary reaction.

This reaction has been studied for more than 50 years. In 1939 Bamford[10] photolyzed NH_3/NO mixtures at 373 K in a series of stationary photolysis experiments. He identified H_2O and N_2 as photolysis products, and proposed a mechanism in which reaction 1a was the loss channel for NH_2. Later work by Serewicz and Noyes[11] in the vicinity of room temperature also identified N_2O as a product of the photolysis; presumably it was destroyed by mercury-sensitized photolysis in Bamford's work, since he made extensive use of mercury seals in his vacuum apparatus. Srinivasan[12] used $^{15}NH_3$ to establish that the N_2O came solely from NO, while the N_2 incorporated one N atom from ammonia and one from nitric oxide, thus ruling out an $NH_2 + NO \rightarrow H_2 + N_2O$ channel. The N_2O was assumed to be formed by the reaction of two HNO radicals, producing N_2O and H_2O. The final "classical" photochemical study was that of Jayanty, Simonaltis, and Heicklen[13] whose actinometric measurements established the quantum yield for formation of N_2 as 1.0 ± 0.1 at 298 K, making $N_2 + H_2O$ the major channel in the reaction of NH_2 with NO at room temperature, since the OH formed in 1b would presumably react with NH_3, producing more NH_2 and increasing the quantum yield above 1.0.

More recently, both the rate and products of the reaction of NH_2 with NO have been the focus of a number of direct determinations between room temperature and ca. 1000 K.[14−37]

* Address correspondence to this author at Mail Stop 9051, Sandia National Laboratories, Livermore, CA 94551.

[†] Present address: Hoffman, Eitle and Partners, Munich, Germany.

[‡] Present address: Beckman Instruments, 2500 Harbor Blvd, Fullerton, CA.

[⊗] Abstract published in *Advance ACS Abstracts,* August 1, 1997.

S1089-5639(97)01316-9 CCC: $14.00

At higher temperatures modeling has been used to determine products of the reaction.[38−40] Portions of the potential energy surface have also been calculated over the past 15 years,[41−46] although all of the thermally accessible stationary points had not been treated before the present work.

Despite the large number of studies of this reaction there were still a number of unresolved issues. None of the previous studies has examined the reactivity or product formation from ND_2, information which will shed additional light onto the mechanism of this complex reaction. All of the thermally accessible stationary points on the potential energy surface had not been calculated at a uniformly high level of theory. In order to understand these reactions better we have undertaken parallel theoretical and experimental studies of this reaction. We have used the G2[47] and G2Q[48] methods to characterize stationary points on the various potential energy surfaces. Experimentally we have used the laser-photolysis/CW laser-induced fluorescence (LP/CWLIF) technique to measure reaction rate coefficients and the discharge flow technique to characterize reaction product branching fractions.

Computational Details

Calculations were carried out using the Gaussian 92[49] and Gaussian 94[50] programs. We used the G2 method, as outlined by Pople and co-workers.[47] G2 uses a series of calculations to approximate a QCISD(T)/6-311+G(3df,2p)//MP2/6-31G(d) calculation with an additional "higher order correction" based on the number of paired and unpaired electrons. The method has been shown to yield atomization energies with a average absolute deviation of 0.9 kcal/mol for a large number of species containing first-row elements. For characterization of potential energy surfaces the empirical "higher order correction" terms cancel, removing that source of empiricism from our calculations. We have carried out additional studies of the applicability of the G2 method to transition state structures[48] and found that it performed well in predicting transition state properties, although its performance for transition states could be enhanced by using QCISD/6-311G(d,p) optimized geometries and frequencies instead of the MP2 optimized geometries and scaled HF frequencies of the G2 method. We have used this G2//QCISD/6-311G(d,p), or G2Q, method to characterize the higher energy (and hence more important) transition states leading to $N_2 + H_2O$ products.

Experimental Section

Reaction Rate Coefficient Measurement. The reaction of NH_2 with NO was investigated using the LP/CWLIF technique. A detailed description of the experimental setup used is given elsewhere[51] and will be discussed only briefly here. Slow flows of highly diluted reagents with argon as buffer gas passed through the reaction zone of a reactor cell, with the reaction zone defined by the perpendicular intersection of the photolysis beam, the CW dye-laser probe beam, and the photomultiplier field of view. Two different types of flow reactors were used during the experiments. For temperatures of $T \geq 292$ K, a heatable quartz reactor with air-cooled window mounts was used, which was resistively heated with a regulated dc power supply. At $T < 292$ K, the experiments were performed in a black-anodized aluminum reaction cell, which was thermostated by circulating cooled methanol through the reactor body. In order to achieve an effective thermal insulation and to avoid water condensation on the reactor windows at low temperatures, both reactors were mounted in an evacuated brass cylinder. The temperature was measured with a chromel−alumel thermocouple directly above the reaction zone. Independent measurements under conditions identical with those used in the experiments showed that the temperature was constant over both the reaction zone and the duration of the experiment within ±2 K above and ±1 K below room temperature, respectively.

NH_2 radicals in their X $^2B_1$ ground state were produced by ArF excimer laser photolysis at 193 nm of NH_3:

$$NH_3 + h\nu \rightarrow NH_2(X\ ^2B_1, A\ ^2A_1) + H\ (^2S) \qquad (2)$$

The quantum yield for production of $NH_2(X^2B_1)$ is 0.97, and only a small fraction ($\Phi = 0.025$) is produced in the (A $^2A_1$) excited state,[52] which undergoes rapid relaxation to the ground state.[18] Although the relaxation of vibrationally excited NH_2 is reported to be fast[24,53] compared to the consumption of NH_2 via reaction 1 under the conditions used, a temperature- and pressure-dependent signal rise time between ≈50 and 300 μs was observed in our experiments without any NO added, which could only be explained by assuming a relatively slow relaxation of rotationally and/or vibrationally excited NH_2 to the equilibrium distribution at the given temperature. Photolyzing ND_3 under the same conditions yielded ND_2 signals with substantially longer rise times. This observation might be explained by the fact that more rotational and vibrational levels can be excited in the ND_2 molecule with the available photolysis threshold energy, which, in turn, may slow down the relaxation process to the equilibrium distribution.

As discussed below, the precursor concentration and photolysis energies needed to be held at relatively low levels, limiting the achievable initial NH_2 concentration. Photolysis pulse energy densities of 2.0−3.0 mJ/cm^2 were used, corresponding to total photolysis energies of 1.6−2.2 mJ/pulse in the quartz cell, and 0.8−1.0 mJ/pulse in the aluminum cell, respectively. The precursor concentrations were $1.2 \times 10^{14} \leq [NH_3] \leq 1.9 \times 10^{14}$ molecules/cm^3. Typical initial NH_2 concentrations were estimated to be $\approx(5 \pm 1) \times 10^{12}$ molecules/cm^3, using the NH_3 absorption coefficient of $\epsilon_{193nm} = 2.91 \times 10^6$ cm^2/mol, given by Atakan et al.[32] Performing experiments with substantially higher NH_3 concentrations and/or photolysis energies led to a systematic decrease of the measured rate constants. Lowering one or both of these quantities below the values used in our experiments did not further change the rate constants but only decreased the S/N of the experiment. Under the experimental conditions used, recombination or disproportionation reactions of NH_2 did not play a significant role based on published reaction rate coefficients.[54] Formation of NH radicals via multiphoton dissociation at 193 nm[52] was avoided by attenuating the photolysis flux density to less than 3 mJ/cm^2. Reactant concentrations were varied in the range $5.4 \times 10^{13} \leq [NO] \leq 58.6 \times 10^{13}$ molecules/cm^3. The total gas flow was adjusted at each temperature to provide a constant flow velocity of about 5 cm/s. This value allowed for full gas exchange between two excimer laser pulses. On the other hand, at this flow velocity the gas mixture could be considered to be stationary during the data acquisition time. Raising or lowering the total gas flow by a factor of 2, leading to flow velocities of 10 and 2.5 cm/s, respectively, did not lead to a change in the measured rate constants. The gas pressure in the cell was held at 10 Torr in all experiments investigating the temperature dependence and the deuterium isotope effect of the title reaction. In an independent evaluation of the pressure dependence of reaction 1 the pressure was varied between 10 and 100 Torr.

The time dependence of $[NH_2]$ was monitored as a function of the NO concentration using the CW LIF technique. CW-laser radiation at $\lambda = 629.91$ nm (Coherent 699-29 ring dye laser, DCM laser dye) was coupled into the cell through a multimode, UV-optical fiber, exciting the (0,8,0) 2_{12} line in the

$A\ ^2A_1 \leftarrow X\ ^2B_1$ electronic transition of NH_2. Fluorescence was observed broad band using a 70 nm fwhm filter centered at 800 nm. At temperatures of $T > 600$ K a 1 nm fwhm filter centered at 632.8 nm was used. This filter shows a considerably higher transmission coefficient at the pump wavelength but is more efficient in cutting off blackbody radiation which is blue-shifted into the detection wavelength region with increasing temperature. ND_2 radicals were pumped at $\lambda = 649.94$ nm, exciting the (0,10,0) 4_{14} and 5_{15} states in the $A\ ^2A_1 \leftarrow X\ ^2B_1$ electronic transition of ND_2, and fluorescence was monitored using a 697 nm high-pass filter.

The measured rate constants were independent of the dye laser power over the range of 100−750 mW output power, measured directly at the dye laser. Approximately 1/2 of the dye laser power was incident on the experiment, due to losses occurring within the optical fiber system. Fluorescence propagating from the probed volume in a downward direction passed through a bandpass filter and was detected by a photomultiplier. The photomultiplier signal was sent to an amplifier/discriminator, and the resulting pulses were counted by a PC microcomputer equipped with a multichannel scaler card. Data were stored throughout 1000 channels with a multichannel scaler dwell time of 10 μs. Signals from 1000 to 5000 excimer laser pulses were summed to generate each NH_2 decay profile. Excimer-laser-induced window fluorescence, fluorescence from $NH_2(A^2A_1)$ formed in the photolysis of NH_3, and chemiluminescence from the reaction $H + NO \rightarrow HNO + h\nu$ partially obscured the NH_2 decay profiles. This interference was removed by using a chopper to block the dye laser on alternate excimer laser pulses and subtracting the signal collected with the probe beam blocked from that with it unblocked.

All reactive experiments were carried out with $[NH_2] << [NO]$. Therefore, pseudo-first-order kinetics apply, and one should expect strictly exponential decays. In the absence of NO the NH_2 decay profiles are dominated by losses due to diffusion and reaction with background impurities, adding some nonexponential character to the measured $[NH_2]$ profiles. We therefore fit the initial slopes of the measured decays to an exponential equation. In this way we generated linear bimolecular plots with intercepts of $\approx 200 \pm 100\ s^{-1}$. These values agree well with the NH_2 losses by diffusion and background reaction one would expect under the experimental conditions used.

Reagents used were NH_3 (Matheson, 99%), ND_3 (MSD Isotopes, 99.4%), NO (Matheson, 98.5%), and Ar (Matheson, 99.9995%). NO was further purified by trap to trap distillation; Ar, NH_3, and ND_3 were used without further purification.

Product Branching Fraction Measurement. The branching fraction measurements were carried out in a discharge flow system with products detected mass spectrometrically. The basic apparatus has been described in some detail earlier.[55] In this study the flow system consisted of three quartz tubes placed inside one another, mounted vertically inside a vacuum jacket made of 45/8 in. Conflat hardware. Tube inner diameters (i.d.) were 21.8, 10.6, and 3.8 mm. This double-injector configuration allowed each of the three tubes to be mounted at different heights from one another and permitted independent variation of the mixing/reacting times in different regions of the system. The outer vacuum jacket was pumped with an oil-free Drystar mechanical pump.

Directly below the concentrically mounted quartz tubes, on the tube axis, sits a 2 mm i.d. skimmer (Molecular Dynamics) which feeds reaction products through a 1.5 mm collimating orifice to a doubly-differentially pumped mass spectrometer. An electron energy of 30 eV and an emission current of 0.75 mA were employed. Relevant ions were pulse counted with an SRS400 gated photon counter interfaced to an computer. Modulated beam sampling was employed to improve signal-to-noise while a liquid nitrogen shroud above the mass spectrometer sampling region considerably reduced background counts.

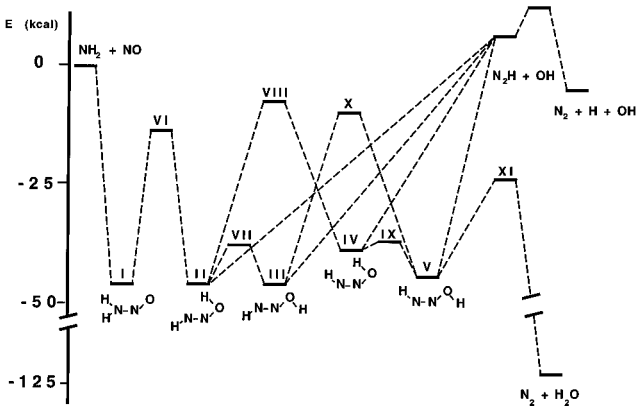

Figure 1. Schematic of the potential energy surface for the $NH_2 + NO \rightarrow$ products reaction, showing the stationary points characterized in this work.

All gas flow rates were controlled and measured with calibrated mass flowmeters while the pressure was monitored with a capacitance manometer and controlled with a butterfly valve connected to an MKS 252 exhaust controller. Flow rates were typically in the range 3−5 m/s while pressure was maintained at 1.0 Torr.

NH_2/ND_2 radicals were formed by reaction of NH_3/ND_3 with F atoms, created by microwave discharging a flowing, dilute solution of F_2/He in a Beenakker-type microwave cavity operating at 50W. The F_2/He mixture passed through the main flow tube, with the NH_3 or ND_3 added through the middle injector. The He/NO/CO mixture was added through the inner injector. The distance between the middle and inner injectors was adjusted to drive the $F + NH_3$ reaction largely to completion. Maximum ammonia concentrations were limited both by formation of solid NH_4F, as well as formation of N_2H_x species, which could be detected mass spectrometrically at $m/e = 30, 31$. We were also restricted to running with $[NH_3]_0 > [F]_0$ in order to minimize formation of NH. The distance between the inner injector and the sampling orifice was adjusted to allow time for the OH + CO reaction to be driven to completion. The NO concentration was set high enough that the $NH_2 + NO$ reaction was largely driven to completion in the mixing plume.

Reagents used were NH_3 (Matheson, 99%), ND_3 (Cambridge Isotope Laboratory), $^{15}N^{18}O$ (Isotec), $^{15}N_2$ (Cambridge Isotope Laboratory, 99%), He (Matheson, 99.9999%), Ar (99.9995%), Ne (Alfa, research grade), 0.5% F_2/He (Matheson, 99.99%), CO (Matherson, 99.99%), CO_2 (Matheson). Typical initial reactant concentrations were, in molecules/cm^3: $[NH_3] = 4 \times 10^{12}$, $[^{15}N^{18}O] = 3.5 \times 10^{13}$, and $[CO] = 1.2 \times 10^{15}$. NH_3, ND_3, $^{15}N^{18}O$, and CO_2 were purified through three freeze−pump−thaw cycles prior to use. Before experiments with ND_3, the flow system was deuterated by passing D_2O through it overnight.

Results and Discussion

Ab Initio Calculations. G2 and G2Q calculations were utilized to characterize the stationary points on the H_2NNO surface. The surface is shown schematically in Figure 1, with energies, geometries, and frequencies of the stationary points collected in Tables 1−4. The energies of the stationary points

TABLE 1: G2 and G2Q Energies[a]

species	E[MP4/6-311G(d,p)][b]	E[QCISD(T)/6-311G(d,p)][b]	Δ(+)[c]	Δ(2df)[c]	Δ(QCI)[c]	Δ(G2)[c]	Δ(HLC)[c]	Δ(ZPE)[c]	G2 energy[b]
I	−185.470 92	−185.466 11	−12.03	−98.26	4.81	−12.78	−45.00	32.22	−185.601 97
II	−185.470 99	−185.468 26	−11.01	−97.60	2.73	−13.08	−45.00	33.31	−185.601 63
III	−185.468 25	−185.465 82	−13.13	−97.11	2.43	−13.01	−45.00	33.22	−185.600 85
IV	−185.459 40	−185.456 53	−10.10	−98.51	2.87	−13.66	−45.00	32.35	−185.591 44
V	−185.470 00	−185.467 57	−11.25	−97.13	2.44	−13.14	−45.00	32.81	−185.601 29
VI	−185.419 18	−185.412 88	−9.94	−99.82	6.30	−12.16	−45.00	27.90	−185.551 91
VI (G2Q)	−185.418 98	−185.413 06	−9.78	−99.72	5.92	−12.34	−45.00	28.53	−185.551 37
VII	−185.453 44	−185.451 32	−12.69	−97.01	2.12	−13.11	−45.00	31.73	−185.587 40
VIII	−185.401 06	−185.397 88	−13.77	−100.22	3.18	−12.97	−45.00	29.38	−185.539 96
VIII (G2Q)	−185.400 69	−185.397 95	−13.14	−100.40	2.74	13.17	−45.00	29.70	−185.543 53
IX	−185.452 85	−185.450 53	−11.11	−97.83	2.32	−13.59	−45.00	31.37	−185.586 70
X	−185.404 48	−185.401 01	−17.08	−99.34	3.47	−12.39	−45.00	29.44	−185.545 39
X (G2Q)	−185.403 64	−185.401 12	−15.92	−99.57	2.51	−12.74	−45.00	29.84	−185.544 51
XI	−185.429 34	−185.423 40	−16.72	−96.40	5.94	−11.83	−45.00	25.22	−185.568 14
XI (G2Q)	−185.429 89	−185.423 87	−15.61	−96.08	6.03	−12.05	−45.00	26.31	−185.566 30

[a] The notation used is as follows: $\Delta(+) = E$[MP4/6-311+G(d,p)] − E[MP4/6-311G(d,p)]; $\Delta(2df) = E$[MP4/6-311G(2df,p)] − E[MP4/6-311G(d,p)]; $\Delta(QCI) = E$[QCISD(T)/6-311G(d,p)] − E[MP4/6-311G(d,p)]; $\Delta(G2) = E$[MP2/6-311+G(3df,2p)] − E[MP2/6-311G(2df,p)] − E[MP2/6-311+G(d,p)] + E[MP2/6-311G(d,p)]; $\Delta(HLC) = -0.19 \times$ number of α valence electrons − $4.81 \times$ number of β valence electrons; Δ(ZPE) = scaled zero-point vibrational energy. G2 energy = E[MP4/6-311G(d,p)] + Δ(+) + Δ(2df) + Δ(QCI) + Δ(G2) + Δ(HLC) + Δ(ZPE) = E[QCISD(T)/6-311G(d,p)] + Δ(+) + Δ(2df) + Δ(G2) + Δ(HLC) + Δ(ZPE). [b] Energies in hartrees. [c] Energies in millihartrees.

TABLE 2: Calculated MP2/6-31G(d) and QCISD/6311G(d,p) Geometries[a]

	I	II	III	IV	V	VI	VI (QCISD)	VII	VIII	VIII (QCISD)	IX	X	X (QCISD)	XI	XI (QCISD)
r(NO)	1.237	1.369	1.396	1.392	1.424	1.290	1.284	1.442	1.500	1.447	1.466	1.587	1.494	1.864	1.856
r(NN)	1.343	1.258	1.252	1.244	1.240	1.287	1.273	1.248	1.201	1.198	1.237	1.183	1.187	1.170	1.163
r(NHa)	1.011	1.029	1.031	1.046	1.041	1.310	1.278	1.035	0.999	0.994	1.042	0.999	0.992	1.150	1.144
r(NHb)	1.019					1.023	1.017								
r(OH)		0.990	0.976	0.990	0.977			0.978	0.986	0.969	0.980	0.979	0.962	0.985	0.966
∠NNO	112.96	110.86	108.27	118.14	111.57	103.08	102.94	108.48	114.31	114.23	113.42	110.65	110.93	89.47	90.83
∠HaNN	115.81	104.84	103.28	112.67	109.87	81.31	80.57	103.52	177.28	178.63	110.82	173.27	175.10	102.09	97.34
∠HbNN	117.77					117.45	117.84								
∠HON		104.98	101.77	108.16	102.75			103.20	103.11	103.63	103.85	99.08	100.66	136.94	128.62
∠HaNNO	167.31	180.00	180.00	0.00	0.00	0.00	0.00	177.54	0.00	0.00	0.06	0.00	0.00	0.01	−2.98
∠HbNNO	10.91					180.00	180.00								
∠HONN		0.00	180.00	0.00	180.00			87.73	0.00	0.00	67.85	180.00	180.00	180.20	138.62

[a] Distances are in Å, angles in deg.

TABLE 3: Calculated Scaled HF/6-31G(d) and QCISD/6-311G(d,p) Frequencies (in cm^{-1}): (A) Protonated Species and (B) Deuterated Speices

I	II	III	IV	V	VI	VI (QCISD)	VII	VIII	VIII (QCISD)	IX	X	X (QCISD)	XI	XI (QCISD)
(A) Protonated Species														
3531	3529	3669	3523	3662	3403	3573	3623	3663	3919	3603	3681	3938	3610	3825
3367	3312	3297	3130	3195	2069	2180	3271	3549	3724	3177	3650	3860	2076	2198
1680	1719	1755	1730	1763	1511	1497	1732	1787	1783	1735	1818	1836	1894	1858
1590	1445	1445	1460	1434	1346	1375	1421	1346	1324	1414	1323	1290	1059	1161
1243	1382	1348	1299	1318	1198	1210	1305	867	776	1286	801	716	1010	981
1116	1015	988	983	1023	1145	1182	959	649	583	985	640	546	767	807
664	964	978	972	946	944	972	952	547	556	920	562	496	550	532
615	659	656	679	635	629	534	666	486	363	647	446	418	106	187
334	596	443	423	423	2182i	2052i	481i	1394i	1427i	413i	1388i	1389i	1442i	1446i
(B) Deuterated Species														
2618	2568	2672	2564	2668		2624	2639		2919	2630		2936		2785
2430	2425	2414	2291	2338		1314	2394		2718	2335		2810		1937
1669	1705	1737	1713	1742		1428	1727		1719	1731		1772		1510
1258	1210	1197	1193	1180		1277	1163		1053	1131		1003		862
1086	1079	1019	995	980		1107	991		731	992		657		806
963	922	909	933	915		908	883		533	882		530		734
563	727	734	789	819		837	700		432	745		359		508
500	582	604	593	562		403	632		282	585		334		141
258	466	335	320	314		1494i	363i		1106i	270i		1074i		1081i

agree well with the limited set calculated by Walch using CASSCF/ICCI,[46] reinforcing our claims for the accuracy of the G2 and G2Q methods. It is also apparent that the lower levels of theory used in earlier work were insufficient to accurately characterize the potential energy surface.

The reaction is initiated by the addition, without barrier, of NH_2 to NO to form an H_2NNO adduct. The adduct is slightly nonplanar, with the hydrogens located about 11° above and below the NNO plane. This adduct undergoes a 1, 3 H-atom transfer to yield a planar HNNOH species. This species can undergo a series of cis−trans isomerizations, giving rise to four distinct HNNOH isomers, II−V, all of which are planar. One of these isomers, V, is configured correctly to undergo a four-center elimination yielding N_2 and H_2O. Additionally, all of

TABLE 4: Energetics of H_2NNO Species[a]

	Casewit and Goddard[41]	Melius and Binkley[42]	Abou-Rachid, et al.[43−44]	Harrison and MacIagan[45]	Walch[46]	this work	experiment
I	−29.8	−48.1	−39.9	−37.0	−44.0	−45.8	
II	−32.0	−47.5		−36.2	−45.7	−45.6	
III	−31.2	−45.5	−38.3	−34.4	−44.5	−45.1	
IV	−24.0	−41.1		−29.2		−39.2	
V	−32.4	−47.2		−36.1	−45.5	−45. 4	
VI		−19.7	0.5	−2.8	−14.4	−14.0(−14.4[b])	
VII				−26.2		−36.7[b]	
VIII				7.8		−6.8(−7.2[b])	
IX				−25.9		−36.2[b]	
X		−7.0		6.5	−7.4	−9.8(−10.3[b])	
XI		−25.2		−7.6	−21.0	−23.4(−24.6[b])	
N_2-H ts + OH		8.7		11.5		10.0(9.9[b])	
N_2H + OH		2.4	−3.5	6.3		4.5	
N_2 + H + O_H		−8.8	−14.7	−13.0		−4.7	−6.5
N_2 + H2O		−134.2	−113.1	−113.2		−122.8	−124.4
^3H_2NNO						4.0	

[a] All energies are in kcal/mol, relative to NH_2 + NO, 0 K, including zero-point energies. Energies are evaluated at G2 level for equilibrium species and G2Q level for transition states, unless otherwise noted. [b] Energy is evaluated at G2 level for transition state.

the HNNOH isomers can undergo an endothermic, barrierless bond fission to yield N_2H and OH. The product branching fraction will depend on the competition between bond fission from the various HNNOH isomers yielding N_2H + OH and passage over the barriers separating H_2NNO and H_2O + N_2. These barriers are of two types, the first transforming *trans*-HNNO species into *cis*-HNNO species, and the second transforming *cis*-NNOH species into *trans*-NNOH species. The first of these isomerizations is accomplished by means of a planar transition state, with a nearly linear NNH moiety. The two transition states of this type, VIII and X, exhibit substantial barriers to the isomerization. The second of these isomerizations is accomplished by a rotation about the NO bond. The two transition states of this type, VII and IX, have low barriers, and we expect the species they connect to be equilibrated.

Rate Coefficient Determination. The reaction rate coefficients of the reaction $NH_2 + NO \rightarrow$ products (1) were measured at 22 temperatures between 203 K ≤ T ≤ 813 K by following the disappearance of NH_2. Initial NO concentrations between 5.41×10^{13} and 58.57×10^{13} molecules/cm^3 were used, yielding pseudo-first-order decay rates, k', between 1126 and 6626 s^{-1}. The experimental conditions and results are summarized in Table 5. The assigned error limits are the 2σ error limits for the 95% confidence intervals of the linear least-square fits. Plots of k' versus [NO] for different temperatures are shown in Figure 2. The data points for each temperature can be described very accurately by a least-squares straight line, giving the bimolecular rate constant $k_1(T)$ as the slope of the line. The nonzero intercepts are due to diffusion and background reactions. The temperature dependence of reaction 1 is shown in Figure 3, where the kinetic data $k_1(T)$ are logarithmically plotted against log (T). The error bars denote the 2σ statistical error limits of the experimental data as given in Table 5. The data over the temperature range 203 ≤ T ≤ 813 K are well represented by a weighted three-parameter fit

$$k_1(T) = 1.65 \times 10^{-7} T^{-1.54} \exp(-93\ \mathrm{K}/T)\ \mathrm{cm}^3/(\mathrm{molecule \cdot s})$$

The data can also be described using a weighted linear fit of the form $k_1 = AT^n$, yielding a rate coefficient of

$$k_1(T) = 2.55 \times 10^{-8} T^{-1.27}\ \mathrm{cm}^3/(\mathrm{molecule \cdot s})$$

The solid line in Figure 3 shows the result of the three-parameter fit.

TABLE 5: Experimentally Measured Rate Coefficients for the Reaction $NH_2 + NO \rightarrow$ Products

T (K)	p (Torr)	[NH_3] (10^{14}/cm^3)	no. of expts	$k_1(T)$ (10^{-11}cm^3/s)
203	10.0	1.49	9	2.91 ± 0.05
210	10.0	1.46	9	2.90 ± 0.06
210	10.0	1.45	9	2.78 ± 0.03
222	10.0	1.42	9	2.59 ± 0.04
242	10.0	1.51	9	2.35 ± 0.03
266	10.0	1.47	9	2.06 ± 0.05
288	10.0	1.46	5	1.82 ± 0.06
292	10.0	1.40	9	1.88 ± 0.01
292	10.0	1.40	7	1.90 ± 0.02
293	10.0	1.24	9	2.00 ± 0.04
295	10.0	1.24	9	1.87 ± 0.02
328	10.1	1.38	7	1.66 ± 0.05
365	10.1	1.39	7	1.50 ± 0.09
403	10.0	1.39	7	1.32 ± 0.09
453	10.7	1.90	7	1.20 ± 0.04
481	10.0	1.42	9	1.01 ± 0.01
498	10.7	1.53	9	0.99 ± 0.03
538	10.0	1.40	10	0.84 ± 0.04
538	10.1	1.52	6	0.77 ± 0.02
546	10.0	1.56−1.59	8	0.81 ± 0.02
575	10.0	1.42	9	0.73 ± 0.03
613	10.0	1.52	9	0.69 ± 0.02
668	10.0	1.51	10	0.61 ± 0.02
731	10.0	1.41	7	0.57 ± 0.04
813	10.4	1.79	7	0.51 ± 0.04

We have also looked for evidence of falloff behavior in the rate constant, performing experiments at pressures between 10 and 100 Torr at room temperature as well as at an elevated temperature of 548 K. NO concentrations were varied between 3.11×10^{13} and 32.60×10^{13} molecules/cm^3, giving pseudo-first-order decay rates, k', in the range between 770 and 3315 s^{-1}. Argon was used as buffer gas in these experiments. The experimental data are summarized in Table 6. Within the experimental error limits, no pressure dependence could be found between 10 and 100 Torr at room temperature or at 548 K.

The reaction of NH_2 with NO has been investigated by several authors over a wide range of experimental conditions.[14−27,31,32,34,36] Our room temperature reaction rate coefficient of $k_1(295\ \mathrm{K}) = (1.9 \pm 0.1) \times 10^{-11}$ cm^3/(molecule·s) is in very good agreement with previously published results obtained from experiments using nondischarge flow techniques. The room temperature rate coefficient determined using the discharge flow technique, approximately 1×10^{-11} cm^3/(molecule·s), is about a factor of

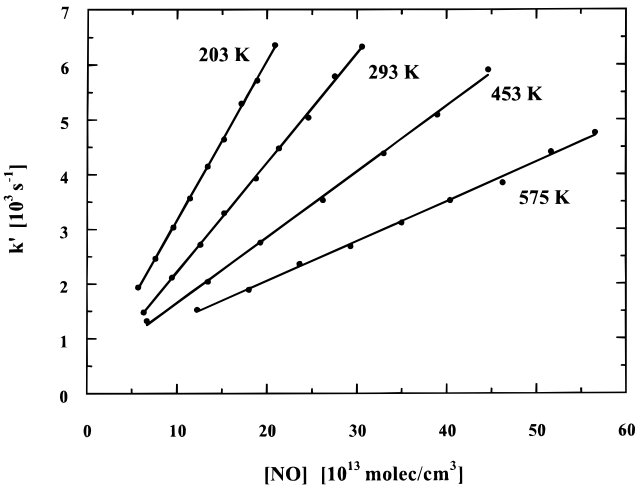

Figure 2. Pseudo-first-order rate coefficients k' for the reaction NH_2 NO → products vs NO concentration at different temperatures.

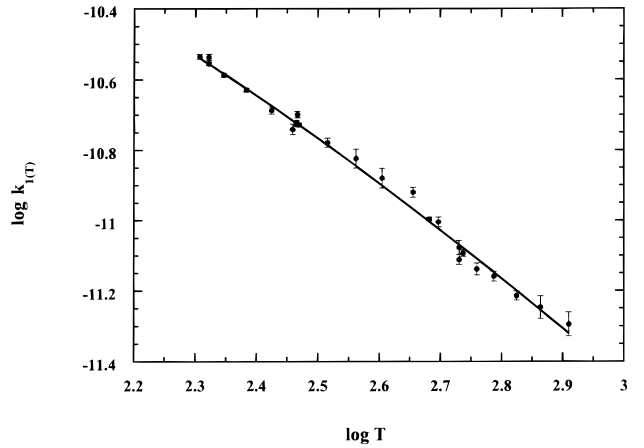

Figure 3. Temperature dependence of the rate coefficient k_1. The error bars give the 2σ error limits for the 95% confidence intervals of the linear least-square fits of the individual $k_1(T)$.

TABLE 6: Pressure Dependence of the Reaction Rate Coefficient for NH_2 + NO → Products

T (K)	p (Torr)	no. of expts	$k_1(T)$ (10^{-11} cm^3/s)
293	20.1	7	1.91 ± 0.02
293	40.0	7	1.89 ± 0.05
293	60.0	6	1.87 ± 0.05
293	80.0	6	1.86 ± 0.08
293	100.0	6	1.90 ± 0.08
546	10.0	8	0.81 ± 0.02
550	100.0	7	0.78 ± 0.08

2 slower than the value determined by other techniques, including this work. The source of this discrepancy is still unclear. Two interesting observations can be made, however. The first is to note that under conditions of high NH_3 concentration or photolysis energy our laser photolysis rates decreased from their asymptotic behavior, which is opposite the behavior normally encountered when secondary chemistry is encountered in photolysis experiments. The second is to note that similar behavior has been observed for the less studied reaction of NH_2 with NO_2, where the flow tube results of Hack et al.[22] are approximately a factor of 2 slower than the results of other workers.[26,31,34,56,57]

The discrepancy between flow tube studies and other studies has been suggested to arise from a stabilized H_2NNO adduct, which can then redissociate in the longer time scales typical of flow tube experiments.[26] Both Gehring et al.,[15] working in the gas phase, and Farber and Harris,[58] studying the reaction of NH_3 with NO over a vanadium oxide catalyst, report seeing m/e = 45 and 46 mass peaks, which they attributed to H_2NNO. However, neither group carried out any isotopic substitution experiments to verify their observations, and we consider it more likely that the peaks are due to $N_3H_3^+$ and $N_3H_4^+$. Foner and Hudson[59] have observed $N_3H_3^+$ and $N_4H_4^+$ in the products of electrodeless discharge hydrazine which had been condensed in a liquid nitrogen trap. At high [NH_2] we have also seen evidence for formation of $N_2H_x^+$ and $N_3H_x^+$ species in our experiments.

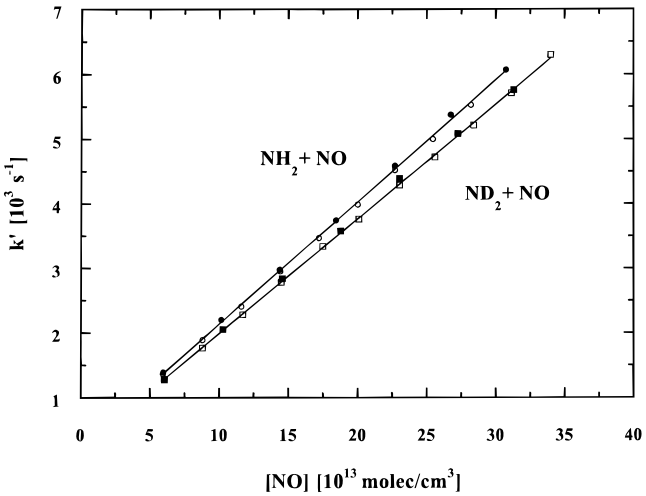

Figure 4. Experimental first-order rate coefficients for the NH_2/ND_2 + NO → products reaction vs the NO concentration at room temperature. Full symbols represent the set of data where ther NH_2 + NO reaction was observed first, and the hollow symbols show the data set beginning with the ND_2 measurements.

The reported temperature dependence of k_1 is complex. It is generally accepted that the reaction rate coefficient decreases between 200 and 1000 K[17,22,23,25,31,32] and is reported to show Arrhenius-like behavior at temperatures above 1680 K.[60] Our observed temperature dependence is in good agreement with that of other workers.

The deuterium isotope effect of the reaction NH_2/ND_2 + NO → products was investigated in this work in the temperature range 210 K ≤ T ≤ 481 K. Typically, experiments using NH_2 as reacting species were perfomed first. Subsequently, the flow system was purged with a mixture of Ar and ND_3 for a waiting period of ≈90 min to allow for isotopic exchange of the ammonia absorbed on the reactor walls before the ND_2 + NO reaction rate was measured. At T = 210 and 292 K the procedure was repeated the following day in reversed order, measuring the ND_2 + NO reaction first. The order of experiments did not show any influence on the observed isotope effect, indicating that the isotopic exchange was completed within the waiting period. This can be seen in Figure 4, where the experimental first-order rate constants of the room temperature experiments are plotted vs the NO concentration. Full symbols represent the set of data where the NH_2 + NO reaction was observed first, and the hollow symbols show the data set beginning with the ND_2 measurements. The observed rate constants are clearly independent of the order in which the rates are measured.

The experimental conditions and results for the kinetic isotope effect experiments are given in Table 7. The errors of the rate coefficients are the 2σ statistical errors of the linear fits to the first-order rate vs concentration plots. These errors were used to calculate the limits of the individual isotope effect values as given in Table 7. The measured isotope effect values are plotted

TABLE 7: Deuterium Kinetic Isotope Effect on the Rate Coefficient for the Reaction $NH_2/ND_2 + NO \rightarrow$ Products

T (K)	isotopic species	$[NX_3]$ (10^{14}/cm^3]	no. of expts	$k_1(T)$ (10^{-11} cm^3/s)	k_H/k_D
210	NH_2	1.45	10	2.78 ± 0.03	
210	ND_2	1.47	8	2.70 ± 0.04	1.03 ± 0.03
210	ND_2	1.47	9	2.84 ± 0.07	
210	NH_2	1.46	9	2.90 ± 0.06	1.02 ± 0.05
292	NH_2	1.40	7	1.90 ± 0.02	
292	ND_2	1.47	7	1.78 ± 0.03	1.07 ± 0.03
292	ND_2	1.47	11	1.78 ± 0.02	
292	NH_2	1.40	9	1.88 ± 0.01	1.06 ± 0.02
481	NH_2	1.42	9	1.01 ± 0.01	
481	ND_2	1.43	9	0.96 ± 0.02	1.05 ± 0.03

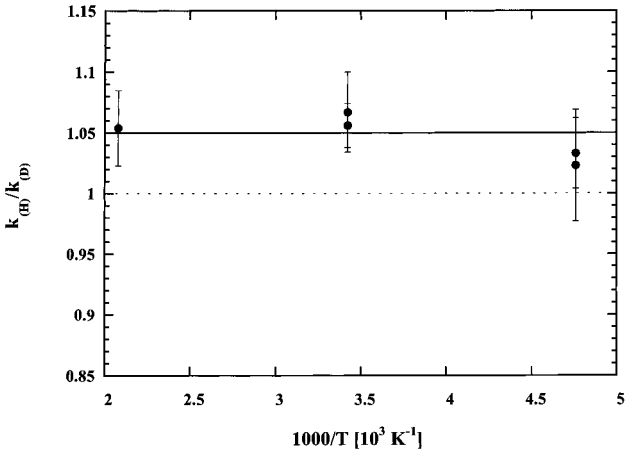

Figure 5. Kinetic isotope effect, k_H/k_D, for the $NH_2 + NO \rightarrow$ products reaction vs temperature.

vs the temperature in Figure 5. Within the experimental error limits the isotope effect is temperature independent for 210 K $\leq T \leq$ 481 K. A weighted average of the experimental data yields an isotope effect of $k_H/k_D = 1.051 \pm 0.012$. Including the estimated systematic errors of the experimental setup, we obtain a final value of the deuterium isotope effect of $k_H/k_D = 1.05 \pm 0.03$.

This is, to our knowledge, the first measurement of the deuterium kinetic isotope effect for this reaction. The small size of the isotope effect is consistent with a barrierless association reaction in which the vibrational frequencies are unchanged at the transition state. Indeed, if we calculate the change in the collision frequency in going from $NH_2 + NO$ to $ND_2 + NO$ we would predict a temperature-independent kinetic isotope effect of 1.04, in excellent agreement with that experimentally observed. This agreement does not rule out other sources of a kinetic isotope effect in this reaction, but it does suggest that they effectively cancel one another out. We also note in passing that several barrierless reactions of CH have large isotope effects,[61,62] highlighting the possible inadequacies of simple treatments of kinetic isotope effects.

Product Branching Fraction. We have measured the product branching fraction, $\Phi = k_{1a}/(k_{1a} + k_{1b}) = [OH]/[N_2]$ for the $NH_2 + NO \rightarrow$ products reaction, as well as the branching fraction for the isotopically substituted reaction of ND_2. To form the NH_2/ND_2 radicals, F atoms formed in the microwave discharge of F_2 were allowed to react with ammonia. Care was taken to prevent formation of NH/ND by monitoring N_2O formation, a known product of NH + NO. Once formed, the NH_2/ND_2 is allowed to mix/react with NO: with the flow rate, [NO] employed, and $k_1 = 1.9 \times 10^{-11}$ cm^3/s, this corresponds three reactive lifetimes. To determine [OH], CO is introduced with NO to completely scavenge the radical:

$$CO + OH \rightarrow CO_2 + H \qquad (3)$$

Determination of $[CO_2]/[N_2]$ yields the desired branching fraction Φ. To separate the CO_2 and N_2 reaction products from background signals, isotopically-labeled $^{15}N^{18}O$ is used, requiring m/e 29 to be monitored for ^{15}NN and m/e 46 for $CO^{18}O$. While the background counts for m/e 46 are low, m/e 29 background is high due to the small but significant amount of ^{13}CO in carbon monoxide. To correct for this, we measure the (m/e 29)/(m/e 28) ratio prior to a reaction run and use this to determine the contribution of ^{13}CO to m/e 29 during a run.

Determination of $CO^{18}O$ and ^{15}NN concentrations is made by measuring a calibrated mixture of $^{15}N_2$ and CO_2. A small mass-dependent transmission correction is determined and applied since the m/e used for the calibrants are different from those in the reaction. Neon and argon are used to determine this correction by measuring the m/e ratio for the two major isotopes, $^{20}Ne/^{22}Ne$ and $^{36}Ar/^{40}Ar$ and comparing to the naturally occurring distribution.

The branching fraction, Φ, at room temperature was $9.0 \pm 2.5\%$ (2σ error) for $NH_2 + NO$ reaction while Φ for $ND_2 + NO$ was measured to be $5.5 \pm 0.7\%$. These results combine to yield the deuterium isotope effect for OH production, $\Phi_H/\Phi_D = 1.6 \pm 0.5$. This is the first measurement of the deuterium isotope effect for OH production, although the room temperature product branching fraction has been measured by numerous workers before.[13,23−25,28−35,37] While early direct measurements of the product branching fraction suggested significant OH production more recent work has settled into the range of $\Phi = 7-10\%$. The present work is thus in excellent agreement with other recent investigations.

This deuterium isotope effect can arise from shifting of barrier heights due to changes in zero point energies and from changes in vibrational sums-of-states occurring upon deuteration. Our ab initio characterization of the stationary points accessible in this reaction allows us to comment on the relative importance of these two factors. To begin with, we will considerably simplify our picture of the potential energy surface. First, we will assume that all of the transition states leading to OH + N_2H can be lumped together. Because these transition states are all loose transition states arising from rotational isomers of the HNNOH adduct this should not represent too large an error. Second, we will consider transition state X as representing the rate-limiting step in the production of $N_2 + H_2O$ products from the HNNOH adduct. Transition state X is the highest energy point on the lowest energy path connecting HNNOH with $N_2 + H_2O$. With these simplifications we can calculate an approximate deuterium isotope effect for the OH producing product channel arising from changes in zero-point energies and arising from changes in sums of states.

Because the OH + N_2H channel is slightly endothermic we expect that the product branching fraction will depend on zero-point energies as

$$\Phi_H/\Phi_D \propto \exp((\Delta E_D - \Delta E_H)/RT)$$

where the ΔE's refer to the difference in zero-point energies between the reactants and OH + N_2H products. Using the results of our G2 calculations, this overall energy difference is

$$\Delta E_D - \Delta E_H = -14 \text{ cm}^{-1}$$

which yields

$$\Phi_H/\Phi_D = 0.93$$

Of course a 14 cm^{-1} difference in calculated zero-point energies is smaller than the anticipated error in this quantity, 70 cm^{-1}.[63] However, a difference of 100 cm^{-1} would be required to yield an isotope effect of the size experimentally observed.

We now turn to a calculation of the size of isotope effect expected from changes in the sum of states. We begin by writing the expression for the branching fraction for production of OH

$$\Phi = k_{1b}/(k_{1a} + k_{1b})$$

The highest point on the minimum energy path for reaction 1a is transition state X; the rate of reaction across this transition state is the limiting process for $N_2 + H_2O$ formation. Thus we assume that the branching fraction can be characterized strictly by considering the branching of adduct III. Recasting in terms of microcanonical rates leads us to

$$\Phi \propto \sum P_{1b}(E)/(\sum P_{1a}(E) + \sum P_{1b}(E))$$

where $\sum P(E)$ is the sum of vibrational states, evaluated using direct count. Note that the term due to the density of states of the adduct cancels out. We further note that $\sum P_{1a}(E) >> \sum P_{1b}(E)$, whichs allows us to write

$$\Phi \propto \sum P_{1b}(E)/\sum P_{1a}(E)$$

$$\Phi_H/\Phi_D \propto [\sum P_{1b}(E)/\sum P_{1a}(E)]_H/[\sum P_{1b}(E)/\sum P_{1a}(E)]_D$$

A final simplification is to note that at the threshold for the $N_2H + OH$ channel $\sum P_{1b}(E) = 1$. We thus arrive at our final, approximate answer

$$\Phi_H/\Phi_D \propto [\sum P_{1a}(E)]_D/[\sum P_{1a}(E)]_H = 1.8$$

This implies that the bulk of the observed deuterium isotope effect is due to the larger sum of states in the $N_2 + D_2O$ channel, relative to the $N_2 + H_2O$ channel.

Conclusion

We have presented results of a combined experimental and theoretical study of the reaction of NH_2 with NO. Accurate ab initio procedures were used to characterize all of the energetically accessible stationary points on the potential energy surface connnecting reactants with products. These calculations provide a framework to understand the results of our experimental measurements of the reaction rate coefficient, its temperature and deuterium isotope dependence, as well as measuring the product branching fraction at room temperature and its deuterium isotope dependence.

Our laser photolysis/CWLIF investigation of the reaction of NH_2 with NO yields a temperature dependent reaction rate coefficient well represented by

$$k_1(T) = 1.65 \times 10^{-7} T^{-1.54} \exp(-93\ \mathrm{K}/T)\ \mathrm{cm}^3/(\mathrm{molecule \cdot s})$$

in the temperature range 203 K $\leq T \leq$ 813 K. An equally accurate description of the data is given by the expression $k_1(T) = 2.55 \times 10^{-8} T^{-1.27}$ cm^3/(molecule·s). The reaction is found to have a weak, temperature-independent deuterium kinetic isotope effect

$$k_H/k_D = 1.05 \pm 0.03$$

in the temperature range 210 K $\leq T \leq$ 481 K.

Using the discharge-flow technique we have measured the product branching fraction for production of OH

$$\Phi_{1b+1c} = 9.0 \pm 2.5\%\ (NH_2 + NO;\ T = 298\ \mathrm{K})$$

$$\Phi_{1b+1c} = 5.5 \pm 0.7\%\ (ND_2 + NO;\ T = 298\ \mathrm{K})$$

The deuterium isotope effect for the product branching fraction, $\Phi_H/\Phi_D = 1.6 \pm 0.5$, is consistent with calculations of the change in the sum of states in the $N_2 + H_2O$ channel caused by deuteration.

Acknowledgment. This work was supported by the Division of Chemical Sciences, Office of Basic Energy Sciences, Department of Energy. We acknowledge the able technical assistance of E. Bochenski and M. Gutzler. M.W. thanks the Deutsche Forschungsgemeinschaft for a research fellowship.

References and Notes

(1) Miller, J. A.; Bowman, C. T. *Progr. Energy Combust. Sci.* **1989**, *15*, 287.
(2) Selgren, S. F.; McLoughlin, P. W.; Gellene, G. I. *J. Chem. Phys.* **1989**, *90*, 1624.
(3) Phillips, L. F. *Chem. Phys. Lett.* **1987**, *135*, 269.
(4) Walch, S. P.; Duchovic, R. J.; Rohlfing, C. M. *J. Chem. Phys.* **1989**, *90*, 3230.
(5) Koizumi, H.; Schatz, G. C.; Walch, S. P. *J. Chem. Phys.* **1991**, *95*, 4130.
(6) McConnell, J. D. *J. Geophys. Res.* **1973**, *78*, 7812.
(7) Roberts, J. M.; Langford, A. O.; Goldan, P. D.; Fehsenfeld, F. C. *J. Atmos. Chem.* **1988**, *7*, 137.
(8) Wayne, R. P. *Chemistry of Atmospheres*, 2nd ed.; Clarendon Press: Oxford, U.K., 1991.
(9) Tyndall, G. S.; Orlando, J. J.; Nickerson, K. E.; Cantrell, C. A.; Calvert, J. G. *J. Geophys. Res.* **1991**, *96*, 20761−20768.
(10) Bamford, C. H. *Trans. Faraday Soc.* **1939**, *35*, 568.
(11) Serewicz, A.; Noyes, W. A., Jr. *J. Phys. Chem.* **1959**, *63*, 843.
(12) Srinivasan, R. *J. Phys. Chem.* **1960**, *64*, 679.
(13) Jayanty, R. K. M.; Simonaltis, R.; Heicklen, J. *J. Phys. Chem.* **1976**, *80*, 433.
(14) Gordon, S.; Mulac, w.; Nangia, P. *J. Phys. Chem.* **1971**, *75*, 2087.
(15) Gehring, M.; Hoyermann, K.; Schacke, H.; Wolfrum, J. *Symp. (Int.) Combust., [Proc.]* **1973**, *14*, 99.
(16) Gordon, S.; Mulac, W. A. *Int. J. Chem. Kinet. (Symp. 1)* **1975**, 289.
(17) Lesclaux, R.; Khe, P. V.; Dezauzier, P.; Soulignac, J. C. *Chem. Phys. Lett.* **1975**, *35*, 493.
(18) Hancock, G.; Lange, W.; Lenzi, M.; Welge, K. H. *Chem. Phys. Lett.* **1975**, *33*, 168.
(19) Sarkisov, O. M.; Cheskis, S. G.; Sviridenkov, E. A. *Bull. Acad. Sci. USSR, Div. Chem. Sci.* **1978**, *27*, 2612.
(20) Roose, T. R.; Hanson, R. K.; Kruger, C. H. *Symp. Int. Shock Tubes Waves Proc.* **1978**, *11*, 245.
(21) Nadtochenko, V. A.; Sarkisov, O. M.; Cheskis, S. G. *Bull. Acad. Sci. USSR, Div. Chem. Sci.* **1979**, *28*, 695.
(22) Hack, W.; Schacke, H.; Schroter, M.; Wagner, H. G. *Symp. (Int.) Combust., [Proc.]* **1979**, *17*, 505.
(23) Silver, J. A.; Kolb, C. E. *J. Phys. Chem.* **1982**, *86*, 3240.
(24) Andresen, P.; Jacobs, A.; Kleinermanns, C.; Wolfrum, J. *Symp. (Int.) Combust., [Proc.*] **1982**, *19*, 11.
(25) Stief, L. J.; Brobst, W. D.; Nava, D. F.; Borkowski, R. P.; Michael, J. V. *J. Chem. Soc., Faraday Trans. 2* **1982**, *78*, 1391.
(26) Whyte, A. R.; Phillips, L. F. *Chem. Phys. Lett.* **1983**, *102*, 451.
(27) Jeffries, J. B.; McCaulley, J. A.; Kaufman, F. *Chem. Phys. Lett.* **1984**, *106*, 111.
(28) Hall, J. L.; Zeitz, D.; Stephens, J. W.; Kasper, J. V. V.; Glass, G. P.; Curl, R. F.; Tittel, F. K. *J. Phys. Chem.* **1986**, *90*, 2501.
(29) Dolson, D. A. *J. Phys. Chem.* **1986**, *90*, 6714.
(30) Silver, J. A.; Kolb, C. E. *J. Phys. Chem.* **1987**, *91*, 3713.
(31) Bulatov, V. P.; Ioffe, A. A.; Lozovsky, V. A.; Sarkisov, O. M. *Chem. Phys. Lett.* **1989**, *161*, 141.
(32) Atakan, B.; Jacobs, A.; Wahl, M.; Weller, R.; Wolfrum, J. *Chem. Phys. Lett.* **1989**, *155*, 609.
(33) Unfried, K. G.; Glass, G. P.; Curl, R. F. *Chem. Phys. Lett.* **1990**, *173*, 337.
(34) Pagsberg, P.; Sztuba, B.; Ratajczak, E.; Sillesen, A. *Acta Chem. Scand.* **1991**, *45*,*329*−334.
(35) Stephens, J. W.; Morter, C. L.; Farhat, S. K.; Glass, G. P.; Curl, R. F. *J. Phys. Chem.* **1993**, *97*, 8944.

(36) Diau, E. W.; Yu, T.; Wagner, M. A. G.; Lin, M. C. *J. Phys. Chem.* **1994**, *98*, 4034.
(37) Park, J.; Lin, M. C. *J. Phys. Chem.* **1997**, *101*, 5.
(38) Kimball-Linne, M. A.; Hanson, R. K. *Combust. Flame* **1986**, *64*, 337−351.
(39) Vandooren, J.; Bian, J.; van Tiggelen, P. J. *Combust. Flame* **1994**, *98*, 402.
(40) Glarborg, P.; Kristensen, P. G.; Dam-Johansen, K.; Miller, J. A. *J. Phys. Chem.*, in press.
(41) Casewit, C. J.; Goddard, W. A., III. *J. Am. Chem. Soc.* **1982**, *104*, 3280.
(42) Melius, C. F.; Binkley, J. S. *Symp(Int.) Combust., [Proc.]* **1984**, *20*, 575.
(43) Abou-Rachid, H.; Pouchan, C.; Chaillet, M. *Chem. Phys.* **1984**, *90*, 243.
(44) Abou-Rachid, H.; Pouchan, C. *J. Mol. Struct.* **1985**, *121*, 299.
(45) Harrison, J. A.; Maclagan, G. A. R.; Whyte, A. R. *J. Phys. Chem.* **1987**, *91*, 6683.
(46) Walch, S. P. *J. Chem. Phys.* **1993**, *99*, 5295.
(47) Curtiss, L. A.; Raghavachari, K.; Trucks, G. W.; Pople, J. A. *J. Chem. Phys.* **1991**, *94*, 7221.
(48) Durant, J. L.; Rohlfing, C. M. *J. Chem. Phys.* **1993**, *98*, 8031.
(49) Frisch, M. J.; Trucks, G. W.; Head-Gordon, M.; Gill, P. M. W.; Wong, M. W.; Foresman, J. B.; Johnson, B. G.; Schlegel, H. B.; Robb, M. A.; Replogle, E. S.; Gomperts, R.; Andres, J. L.; Raghavachari, K.; Binkley, J. S.; Gonzalez, C.; Martin, R. L.; Fox, D. J.; Defrees, D. J.; Baker, J.; Stewart, J. P.; Pople, J. A. *Gaussian 92*; Revision B; Gaussian, Inc.: Pittsburgh, PA, 1992.
(50) Frisch, M. J.; Trucks, G. W.; Schlegel, H. B.; Gill, P. M. W.; Johnson, B. G.; Robb, M. A.; Cheeseman, J. R.; Keith, T.; Petersson, G. A.; Montgomery, J. A.; Raghavachari, K.; Al-Laham, M. A.; Zakrzewski, V. G.; Oritz, J. V.; Foresman, J. B.; Cioslowski, J.; Stefanov, B. B.; Nanayakkara, A.; Challacombe, M.; Peng, C. Y.; Ayala, P. Y.; Chen, W.; Wong, M. W.; Andres, J. L.; Replogle, E. S.; Gomperts, R.; Martin, R. L.; Fox, D. J.; Binkley, J. S.; Defrees, D. J.; Baker, J.; Stewart, J. P.; Head-Gordon, M.; Gonzalez, C.; Pople, J. A. *Gaussian 94*, Revision B.1; Gaussian, Inc: Pittsburgh, PA, 1995.
(51) Durant, J. L.; Tully, F. P. *Chem. Phys. Lett.* **1989**, *154*, 568.
(52) Donnelly, V. M.; Baronavski, A. P.; McDonald, J. R. *Chem. Phys.* **1979**, *43*, 283.
(53) Xiang, T. X.; Gericke, K. H.; Torres, L. M.; Guillory, W. A. *Chem. Phys.* **1986**, *101*, 157.
(54) Mallard, W. G.; Westley, F.; Herron, J. T.; Hampson, R. F.; Frizzell, D. H. *Chemical Kinetics Database*; 5.0 ed.; NIST Standard Reference Data: Gaithersburg, MD, 1993.
(55) Durant, J. L. *J. Phys. Chem.* **1994**, *98*, 518.
(56) Kurasawa, H.; Lesclaux, R. *Chem. Phys. Lett.* **1979**, *66*, 602.
(57) Xiang, T.-X.; Torres, L. M.; Guillory, W. A. *J. Chem. Phys.* **1985**, *83*, 1623.
(58) Farber, M.; Harris, S. P. *J. Phys. Chem.* **1984**, *88*, 680.
(59) Foner, S. N.; Hudson, R. L. *J. Chem. Phys.* **1958**, *29*, 442.
(60) Roose, T. R.; Hanson, R. K.; Kruger, C. H. *Symp. (Int.) Combust., [Proc.]* **1981**, *18*, 853.
(61) Taatjes, C. A. *J. Phys. Chem.* **1996**, *100*, 17840.
(62) Thiesemann, H.; MacNamara, J.; Taatjes, C. A. *J. Phys. Chem.* **1997**, *101*, 1881.
(63) Pople, J. A.; Scott, A. P.; Wong, M. W.; Radom, L. *Isr. J. Chem.* **1993**, *33*, 345.